

Slave-rotor theory on magic-angle twisted bilayer graphene

Shin-Ming Huang,¹ Yi-Ping Huang,² and Ting-Kuo Lee¹

¹*Department of Physics, Center of Crystal Research,
National Sun Yat-sen University, Kaohsiung 80424, Taiwan*

²*Condensed Matter Theory Group, Paul Scherrer Institute, CH-5232 Villigen PSI, Switzerland*
(Dated: February 19, 2022)

We investigate the correlated electrons in the magic-angle twisted bilayer graphene by using the slave-rotor mean-field theory. Owing to the extended figure of Wannier orbitals, we study the two-orbital cluster Hubbard model with spin-valley fourfold degeneracy, focusing around half filling of valence bands below the neutrality point. The theory predicts multiple Mott insulator phases at fractional fillings not only for integer charges per moiré site, and it demonstrates that long-range electron hopping is highly suppressed because multiple-charge excitations are induced. Furthermore, the Kekulé valence bond order is investigated and is found to extend the Mott insulator phases to occupy a finite doping region. Adjacent to Mott insulator phases, superconducting domes emerges by virtue of spin-valley fluctuations. This work has provided a primal understanding and interesting phenomena of the correlated system, and for its novel interaction the model might produce plenty of possibilities waiting to be explored.

I. INTRODUCTION

Recently twisted bilayer graphene (TBG) has aroused considerable interest since the discovery of strongly correlated insulating states and superconductivity^{1,2}. It is quite surprising that strongly-correlated phenomena could emerge from the carbon atoms which have weak interaction effect comparing with strongly-correlated transition metal ions. The successful fabrication of TBG and its novel phenomena opens another route of promising applications in van der Waals heterostructures³. Owing to a weak van der Waals force tying them, two graphene flakes are manipulable to stack with a relative twist angle, giving rise to a long-period moiré superlattice. The moiré lattice parametrized by the twist angle infers a tendency of moiré band narrowing, and theory predicts extremely flat bands can emerge at magic angles⁴⁻⁸. At the magic angle $\theta^* \approx 1.05$, the moiré lattice constant is $a = 13$ nm, and the charge density required to fill a moiré band (including degeneracy from spin and valley) is as low as $n_s \approx 2.6 \times 10^{12}$ cm⁻². The low-energy bands have a bandwidth of the order of 10 meV², serving as an unstable ground against electron-electron interaction.

A great advantage in TBG to investigate the electronic structure is the controllable carrier concentration that experiment can access major part of the phase diagram simply by electronic gating due to a low density of the moiré band. In transport studies, correlated gaps at partial band fillings have been experimentally observed^{1,2,9-13}. With doping, superconductivity appears and resides on either side of the correlated insulating phase as superconducting domes in the temperature-density phase diagram, reminiscent of strongly correlated high- T_c superconductors¹⁴. In addition, the quantum oscillations display vanishing of Fermi surfaces and an increase of the effective mass when the correlated insulating phase is approached, signifying a doped Mott insulator^{1,2}. Through analyzing temperature behavior as well as the magnetic response in conductance², the Mott gap (correlated gap)

was estimated to be 0.3 meV. In comparison with the bandwidth, the small Mott gap reveals that the system might be in close proximity to the Mott transition point. Although there are many features corresponding to Mott physics, some observations conflict our understanding: the phase diagram is quite asymmetric on two doping sides of the Mott insulator phase and the Landau fan suggests broken spin-valley symmetry^{1,2,13}. Nevertheless, TBG as an unconventional superconductor is evident for its relative high critical temperature $T_c \sim 2$ K^{1,13}. To dates, most theoretical studies on superconductivity belong to the weak coupling theories¹⁵⁻²⁴, and a theory in an intermediate-coupling or a strong-coupling regime is requisite^{16,25-29}.

In this work, we investigate TBG as a doped Mott insulator by the cluster Hubbard model proposed in Refs. 30 and 31. The theory is developed based on the peculiar extended Wannier orbitals^{30,31} where the electron repulsion is a cluster charge (total charge in a hexagon) interaction. Studying such a model with unconventional interaction is challenging because of the non-trivial low-energy constraint on a cluster. To conquer the difficulty, we use the slave-rotor approach to deal with the correlation effects. The strategy has been used widely in the study of correlated strongly spin-orbit coupled materials^{32,33}, but the difference in our method is that the rotor in this work is to depict total charge in a hexagon instead of on a single site. Utilizing the slave-rotor mean-field theory and comparing different approximations, we can simplify the problem and discover a number of interesting phenomena in the model. Distance-dependent renormalization effects on hopping appear plainly due to the cluster interaction. Therefore, a short-range hopping model becomes sufficient in the strong coupling regime so that the critical value of interaction for the Mott transition becomes less sensitive to the details of the bare band structure. Most notably, the Mott insulator phase appears, if happens, not only at integer fillings (charges per moiré) but also at fractional ones as $2 \pm 1/3$ and so on. We also found the

system having a tendency of the Kekulé valence bond order (KVB)^{27,34} thanks to the slave-rotor representation. The KVB is found to be compatible with the Mott insulator phase, exhibiting a Kekulé valence bond solid. Considering spin-valley fluctuations, the model can realize superconducting pairing and gives a phase diagram similar to experimental observations.

The paper is organized as follows. Section II shows the Hamiltonian. Section III demonstrates the slave-rotor theory and discusses the Mott transition. Three approximations are studied: i) the single-site approximation in Sec. III A, ii) two-site approximation in Sec. III B, and iii) the O(2) nonlinear sigma model in Sec. III C. (Reader who are familiar with the theory and approximations can skip the detail and just refer to the conclusive result in Fig. 3.) Section IV discusses the phase diagram of antiferromagnetic and superconducting orders. In Sec. V, the Kekulé order and its effect to the Mott transition are shown. Finally, we conclude the work in Sec. VI. Some details of derivation are found in Appendix: the local gauge symmetry in the slave-rotor representation in Appendix A, and the mean-field Hamiltonian for hopping and the nonlinear sigma model in Appendix B and C, respectively.

II. THEORETICAL MODEL

The flat bands of TBG are constructed by the low-energy states at valleys K and K' from two graphene layers. The two valleys are considered as independent degrees of freedom when the twist angle is small. Although the electrons from the flat bands in TBG are seen to concentrate on the AA sites forming a triangular lattice, developing a tight-binding model for a low-energy effective theory could be subtle. One cannot describe the system by an effective tight-binding model on a triangular lattice since it is unable to produce Dirac points due to symmetry reason^{30,31,35}. Instead, the effective model should be based on Wannier orbitals on honeycomb-lattice sites (BA and AB sites). Theoretical studies report that two Wannier orbitals from BA and AB sites look like fidget-spinner orbitals that their distributions peak on three adjacent hexagon centers (AA sites)^{30,31,35} [refer to Fig. 1(b)]. The Wannier orbitals, respecting C_3 rotational symmetry, show equal amplitude but $\pm 2\pi/3$ phase differences on three adjacent sites; in other words, two Wannier orbitals at valley K have angular momentum of -1 , while the other two at valley K' take angular momentum of $+1$ because of time-reversal symmetry.

Based on these Wannier orbitals, a hopping Hamiltonian is written as

$$H_t = \sum_{ij} \sum_{\kappa=\pm} \sum_{\sigma=\uparrow,\downarrow} (t_{\kappa,ij} - \mu\delta_{ij}) c_{\kappa i\sigma}^\dagger c_{\kappa j\sigma}, \quad (1)$$

where κ and σ denote valley and spin states, respectively, and two sublattices are implicit in the site notation and

will be specified by A and B later. Because of time-reversal symmetry, hopping integrals $t_{\kappa,ij} = t_{\bar{\kappa},ij}^*$. We will adopt the hopping integrals constructed by Koshino et al. subjected to maximally localized Wannier orbitals at the magic angle θ^* . We consider only hopping up to fifth nearest neighbors ($r = \sqrt{3}a$) unless specified otherwise. For convenience, we will name the n -th nearest neighbor (nNN) hopping integral t_n ($n = 1, \dots, 5$). Although it was noted that to capture a better band structure at high energies, long-range hopping integrals were small but required, we will show in this work that electronic correlation, giving different order of renormalization, will highly reduce long-range hopping.

Referring to Fig. 1(b) and imagining that a lobe of a Wannier orbital takes charge of $e/3$ and concentrates completely at the center of a hexagon, Wannier orbitals can overlap between onsite, 1NN, 2NN, and 3NN sites with numbers of lobes in 3:2:1:1. Since Wannier orbitals at the corners of a hexagon extends to the center of the plaquette, the electrons on the six corners will interact through the wave function overlap at the center of the plaquette. In the approximation that the interaction occurs only at the overlapping region, the number of lobes at a plaquette center will determine the interaction at that hexagon. As a result, the cluster interaction is introduced as

$$H_U = U \sum_{i_c} (Q_{i_c} - C)^2, \quad (2)$$

where i_c runs over hexagon sites (the subscript c is for the hexagonal cluster), the hexagon charge $Q_{i_c} = \sum_{j \in i_c} n_j$ is the particle number of six sites in the hexagon ($n_j = \sum_{\kappa,\sigma} c_{\kappa j\sigma}^\dagger c_{\kappa j\sigma}$ includes two spins and two valleys), and C is the charge reference. In this work, we are interested in the region around the Mott insulator phase at half filling of valence bands below neutrality, where there is one electron per lattice site. So we take $C = 6$ and call the case undoped. When a hexagon has five or seven particles, it gets an energy of U . Our model for the system is

$$H = H_t + H_U. \quad (3)$$

It is estimated that the system could enter the strong correlation regime, so that the low-energy states are confined to a restricted Hilbert space in the $U/t \rightarrow \infty$ limit. Rather than no doubly occupied site in the Hubbard model, the present interaction, in some sense, demands a weaker constraint: six particles in a hexagon. This leads to high degeneracy²⁶ and high dimensions of the restricted Hilbert space, in which more configurations are allowed; for instance, a hexagon can be of no holon (empty site) and no doublon (doubly occupied site), one, two, or three holon-doublon pairs, not to mention spin and valley configurations. Nevertheless, the present one exhibits Mott physics as well, since any particle's movement brings about changes of hexagon charges nearby (see Fig. 2) that is unlikely to happen because of an $\mathcal{O}(U)$ energy cost.

III. SLAVE ROTOR THEORY OF THE MOTT TRANSITION

To deal with the degenerate problem, we adopt the slave-rotor representation^{36,37} in which an electron operator c_{σ}^{\dagger} is written in terms of the spinon (auxiliary fermion) f_{σ}^{\dagger} and the rotor θ conjugate to some charge (or angular momentum). Different from the original setting^{36,37}, the charge we concern is the hexagon charge, so we define the angular momentum $L_{i_c} = Q_{i_c} - 6$ that equates the hexagon charge relative to six. Because three hexagons meet at a sublattice site, an electron operator for any site needs three rotors for adjoining hexagons. Considering that the lattice is bipartite, we define operators on site A and B as

$$\begin{aligned} c_{A\kappa i\sigma}^{\dagger} &= f_{A\kappa i\sigma}^{\dagger} \prod_{l=1,2,3} e^{i\theta_{i-d_l}}, \\ c_{B\kappa i\sigma}^{\dagger} &= f_{B\kappa i\sigma}^{\dagger} \prod_{l=1,2,3} e^{i\theta_{i+d_l}}, \end{aligned} \quad (4)$$

where $\mathbf{d}_{1,2,3}$ are three vectors connecting nearest neighbor (NN) A and B sites [see Fig. 1(a)], and $e^{\pm i\theta_{i_c}}$ will increase (decrease) the quantum number of L_{i_c} by one, i.e. $[L_{i_c}, e^{\pm i\theta_{i_c}}] = \pm e^{\pm i\theta_{i_c}} \delta_{i_c, i'_c}$. The slave rotor formalism here is designed for the specific filling. Unlike conventional slave-rotor approach where single fermion Hilbert space on site i is enlarged into $\mathcal{H}_i(i) \rightarrow \mathcal{H}_{\text{spin}}(i) \otimes \mathcal{H}_{\text{rotor}}(i)$. The representation is designed such that the cluster energy of the full many-body fermion wave function is captured by bosonic $U(1)$ rotors, $e^{i\theta_{i_c}}$, defined on center of plaquettes. Using this representation, we don't have the conventional $U(1)$ gauge redundancy in contrast with slave-rotor approach for various Hubbard models. The local gauge symmetry is discussed in Appendix A.

Taking Eq. (4) into H_t , one observes that there are different numbers of phase factors in it by referring to Fig. 2. The NN hopping brings out two phase factors like $e^{i\theta_{i_c} - \theta_{i'_c}}$ for one hexagon loses a charge and another increases one. Differently, the 2NN and 3NN hoppings introduce four phase factors. For rest hoppings of longer distance, six phase factors show up. It is this complicated H_t in the slave-rotor representation that makes the solving difficult.

The interaction H_U , on the other hand, is written as $H_U = U \sum_{i_c} L_{i_c}^2$. In order to impose the constraint on L_{i_c} , we add

$$H_h = h \sum_{i_c} \left(L_{i_c} - \sum_{j \in i_c} \sum_{\kappa, \sigma} f_{\kappa j \sigma}^{\dagger} f_{\kappa i \sigma} + 6 \right), \quad (5)$$

to H , where h is a Lagrange multiplier determined by optimization, and call the total $H' = H + H_h$. Considering the particle number constraint,

$$\sum_{\kappa, \sigma} \langle f_{\kappa i \sigma}^{\dagger} f_{\kappa i \sigma} \rangle = \sum_{\kappa, \sigma} \langle c_{\kappa i \sigma}^{\dagger} c_{\kappa i \sigma} \rangle = 1 + \frac{x}{2}, \quad (6)$$

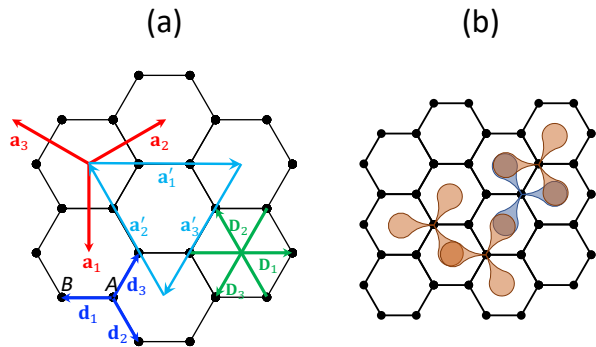


FIG. 1. (a) Moiré superlattice of the TBG: sublattices A and B and 1NN vectors \mathbf{d}_l ($l = 1, 2, 3$), 2NN as well as primitive vectors \mathbf{a}_l , and 3NN vectors \mathbf{D}_l . These vectors are related by $\mathbf{d}_l = \frac{1}{3}(\mathbf{a}_{l-1} - \mathbf{a}_{l+1})$ and $\mathbf{D}_l = -2\mathbf{d}_l$. The 5NN vectors $\mathbf{a}'_l = \mathbf{a}_{l+1} - \mathbf{a}_{l-1}$ will be unit vectors for the Kekulé valence bond order. We identify subscripts $l \equiv l \pmod{3}$ in this paper, for instance $\mathbf{d}_4 \rightarrow \mathbf{d}_1$. (b) Illustration of Wannier orbitals and their overlap with neighbors. A lobe of a Wannier orbital takes charge of $e/3$.

Eq. (5) becomes the constraint

$$\langle L_{i_c} \rangle = 3x \quad (7)$$

in the mean-field level. Here x is the doping concentration, and $x > 0$ ($x < 0$) is for electron (hole) doping.

We will solve the model in the slave-rotor representation by using the mean-field theory to decouple the rotor and the spinon sectors as $H' = H_{\theta}^{\text{MF}} + H_f^{\text{MF}}$, by which the electron ground-state wave function is the product of those of two sectors $|\Psi\rangle = |\Psi_{\theta}\rangle |\Psi_f\rangle$ subject to the constraints in Eqs. (6) and (7). The decoupled H_{θ}^{MF} is not solvable can not be solved exactly. We self-consistently solve it by three approximation methods: the single-site, two-site approximation, and the $O(2)$ nonlinear sigma model and discuss our solutions in the following sections.

A. Single-site approximation

The single-site approximation is a cluster mean-field theory which approximates that rotors in different clusters are independent and they interact with the mean-field environment to gain self-energies³⁷. Here the cluster has only one site. We emphasize that the "site" is for the rotor as a position of a hexagon when discussing single-site and two-site approximations. The mean field turns out to be the rotor's condensate fraction $\sqrt{Z} \equiv \langle e^{i\theta_{i_c}} \rangle$ and it has no spatial correlation, e.g. $\langle e^{i\theta_{i_c}} e^{-i\theta_{j_c}} \rangle \approx \langle e^{i\theta_{i_c}} \rangle \langle e^{-i\theta_{j_c}} \rangle = Z$. (We choose a real gauge $Z \geq 0$.) Using $\prod_{i=1}^m e^{i\theta_i} e^{-i\theta_{i'}} \approx m Z^{m-1/2} (e^{i\theta_i} + e^{-i\theta_i})$, we have

$$H_{\theta}^{\text{MF}(1)} = K (e^{i\theta_{i_c}} + e^{-i\theta_{i_c}}) + U L_{i_c}^2 + h L_{i_c}, \quad (8)$$

where implicit summation over i_c is taken, $K = (\sqrt{Z} \sum_j' + 2\sqrt{Z^3} \sum_j'' + 3\sqrt{Z^5} \sum_j''') K_{ij}$ from mean-field of H_t with $K_{ij} = \sum_{\kappa} t_{\kappa,ij} \chi_{ij}^{\kappa} + \text{c.c.}$ and $\chi_{ij}^{\kappa} \equiv \sum_{\sigma} \langle f_{\kappa i \sigma}^{\dagger} f_{\kappa j \sigma} \rangle$ which renormalization factors depend on distance of ij so we decouple them by \sum_j' , \sum_j'' , and \sum_j''' as we elaborated before. We replace χ_{ij}^{κ} by χ_n^{κ} when ij are nNN sites and the same for K_n . When we consider hopping up to 5NN bonds, $K = 3\sqrt{Z}M$ with

$$M = (K_1 + 4ZK_2 + 2ZK_3 + 6Z^2K_4 + 6Z^2K_5). \quad (9)$$

Equation (8) is reduced to a single-site problem, and Z and h have to be determined self-consistently. Starting by initializing K and h , we write Eq. (8) in the eigenbasis of L , $|n_{\theta}\rangle$, in which $e^{i\theta i_c}$ becomes off-diagonal. Numerically, a truncated Hilbert space of $|n_{\theta}| \leq n_{\text{truncate}}$ is used, which is justified if the results are weakly susceptible to n_{truncate} . After diagonalizing and obtaining the ground state of Eq. (8), new $Z = \langle e^{i\theta i_c} \rangle^2$ and hence K are generated to update Eq. (8). Therefore, it is an iterative procedure to find K or Z until convergence. Meanwhile, one needs to tune h as well so as to maintain Eq. (7). As for $\langle f_{\kappa i \sigma}^{\dagger} f_{\kappa j \sigma} \rangle$ in K , they are evaluated from the ground state of the spinon sector, which similarly depends on Z learned from the rotor sector.

The mean-field Hamiltonian of the spinon reads

$$H_f^{\text{MF}(1)} = \sum_{ij} \sum_{\kappa, \sigma} (t_{\kappa,ij}^{\text{eff}} - \mu^{\text{eff}} \delta_{ij}) f_{\kappa i \sigma}^{\dagger} f_{\kappa j \sigma}. \quad (10)$$

Similarly, some parameters in H_f^{MF} are answered by the rotor. The effective chemical potential is shifted to be $\mu^{\text{eff}} = \mu + 3h$, and the hopping t_{ij}^{eff} are renormalized by degrees of the rotor, giving $t_{ij}^{\text{eff}} = \{Z, Z^2, Z^3\} t_{\kappa,ij}$ for different distances. Specifically, $t_{\kappa,1}^{\text{eff}} = Z t_{\kappa,1}$, $t_{\kappa,2(3)}^{\text{eff}} = Z^2 t_{\kappa,2(3)}$, and $t_{\kappa,4(5)}^{\text{eff}} = Z^3 t_{\kappa,4(5)}$. One solves the ground state of Eq. (10) with a proper μ^{eff} under the particle-number constraint in Eq. (6). The resulting $\langle f_{\kappa i \sigma}^{\dagger} f_{\kappa j \sigma} \rangle$ here are used to revise those in Eq. (8). Once again, one returns to the rotor section and solves until convergent.

Figure 3 shows Z (single-site), by the black dotted line, as a function of U in the undoped case. The condensate fraction $0 \leq Z \leq 1$ turns out to be the quasiparticle coherent weight. With increase of U , Z decreases and becomes zero when U is larger than the critical value $U_c \approx 2.8$ meV, above which the system enters the Mott insulator phase. However, the observed value of U_c is much smaller than the expected value which should be about the bandwidth of the noninteracting electronic system of 7.35 meV in the present model. We also calculated the system with hopping with distance longer than the 5NN site ($r > \sqrt{3}a$), and found an identical U_c without prominent change in Z (not shown). Figure 4 shows the dressed bands ($Z = 0.205$), which resembles a graphene-like one, compared to the bare bands ($Z = 1$),

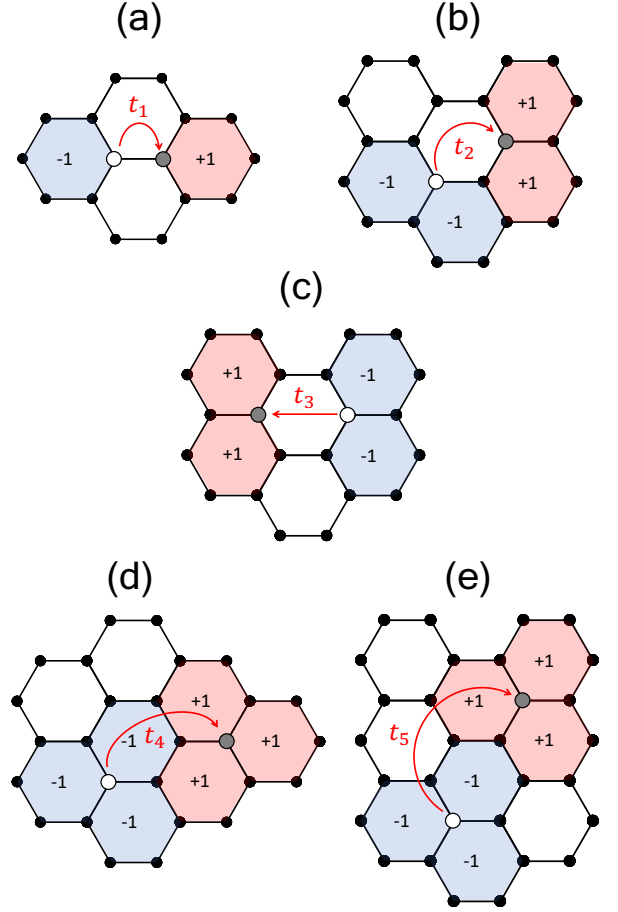


FIG. 2. Schematic illustration of hexagon charge variation (± 1) due to electron hopping. (a)-(e) are for 1NN, 2NN, 3NN, 4NN, and 5NN hoppings, respectively. When a hexagon increases (decreases) its charge by one, a rotor factor $e^{i\theta}$ ($e^{-i\theta}$) is introduced. So the hopping renormalization factor in the single-site approximation is $Z = \langle e^{i\theta} \rangle \langle e^{-i\theta} \rangle$ in (a), Z^2 in (b,c), and Z^3 in (d,e).

clearly showing nonuniform band renormalization as seen in $H_f^{\text{MF}(1)}$. The result justifies it feasible to neglect long-range hopping terms and suggests that the effective hopping is much shorter with the cluster interaction.

B. Two-site approximation

In the previous single-site approximation, the quasiparticle weight Z controls the effective hopping of spinons (t_{ij}^{eff}) and hence the bandwidth renormalization Z_{BW} (defined as the ratio of the four-band bandwidth at finite U to that at zero U). However, it is unphysical that the spinon band becomes completely flat in a Mott insulator phase because quantum fluctuations can still mediate nonlocal correlations. Therefore, we have to include spa-

tial corrections among rotors that $\langle e^{i\theta_{i_c}} e^{-i\theta_{i'_c}} \rangle \neq 0$ even in the absence of condensation, which fixes effective hopping amplitudes of the spinon. This inclusion will solve the problem accordingly, giving finite Z_{BW} for all finite U .

We enlarge the cluster to two sites to allow the coupling between two rotors³⁸. According to Fig. 2(a), a NN hopping of an electron creates nonadjacent rotor excitations, suggesting no correlation between adjacent rotors. So to decide a two-site cluster, we choose the two sites with one at i_c and the other at $i'_c = i_c + \mathbf{a}'_2$ (we select one of three directions). To perform the two-site approximation, we single out terms in H_t associated with the target cluster and contract spinon hoppings by χ_n^κ wherein. Then, we do the mean field procedure by contracting spinons as $\sum_\sigma f_{\kappa i \sigma}^\dagger f_{\kappa j \sigma} \rightarrow \chi_{ij}^\kappa$ and rotors not in the cluster as $e^{i\theta_{j_c}} \rightarrow \sqrt{Z}$. Consequently, the two-site Hamiltonian of the rotor is

$$\begin{aligned} H_\theta^{\text{MF}(2)} = & \frac{1}{2} M \left(e^{i\theta_{i_c}} e^{-i\theta_{i'_c}} + \text{H.c.} \right) \\ & + \frac{5}{2} \sqrt{Z} M \left(e^{i\theta_{i_c}} + e^{i\theta_{i'_c}} + \text{H.c.} \right) \quad (11) \\ & + U \left(L_{i_c}^2 + L_{i'_c}^2 \right) + h \left(L_{i_c} + L_{i'_c} \right), \end{aligned}$$

where summation over i_c is also omitted and M is defined in Eq. (9). (One can check that $H_\theta^{\text{MF}(2)}$ becomes $H_\theta^{\text{MF}(1)}$ exactly by doing the single-site approximation on it.) Numerically, we will solve the ground state in the basis of $|n_\theta, n_{\theta'}\rangle$. Because of the coupling of rotors in Eq. (11), we have the spatial correlation $Z_1 \equiv \langle e^{i\theta_{i_c}} e^{i\theta_{i'_c}} \rangle$ possibly different from Z .

For the spinon Hamiltonian $H_f^{\text{MF}(2)}$, it is quite similar to $H_f^{\text{MF}(1)}$ but changes the effective hopping integrals as $t_{\kappa,1}^{\text{eff}} = Z_1 t_{\kappa,1}$, $t_{\kappa,2(3)}^{\text{eff}} = Z_1^2 t_{\kappa,2(3)}$, and $t_{\kappa,4(5)}^{\text{eff}} = Z_1^3 t_{\kappa,4(5)}$. Similar to what elaborated in Sec. III A, values of Z and h in $H_\theta^{\text{MF}(2)}$ and values of Z_1 and μ^{eff} in $H_f^{\text{MF}(2)}$ are solved self-consistently. The result of Z_1 is shown in Fig. 3 by the red dashed line. One can observe that the one-site and two-site approximations have very close U_c . For the latter, the spatial correlation Z_1 at $U < U_c$ is contributed mainly from the condensate, and its noncondensate part is maximal at U_c .

C. Nonlinear sigma model with Hartree-Fock mean field theory

The last approximation we are going to show is the nonlinear sigma model with minimal dynamical fluctuations. We replace $e^{-i\theta_{i_c}}$ in H' by the complex bosonic field X_{i_c} with the size constraint $|X_{i_c}|^2 = 1$, which is imposed by a Lagrangian multiplier, λ . This representation transforms the rotor section into an O(2) nonlinear sigma model in which the angular momentum is the source of

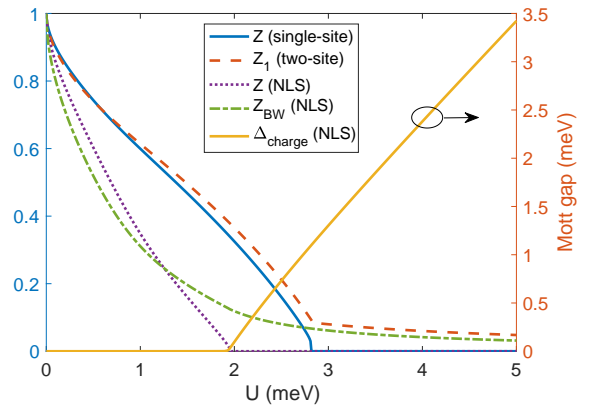


FIG. 3. Plot of the quasiparticle weight (rotor condensation amplitude) Z , the bandwidth renormalization Z_{BW} , and the Mott gap Δ_{charge} as a function of $U = 5$ meV in the undoped system ($x = 0$). Except the dotted line, which is obtained in the single-site approximation, the rest include spatial correlations.

dynamical fluctuations of X . The model can be generalized to an O(2N) model by extending the bosonic field to an N -component complex field $X_{i_c, \alpha}$ ($\alpha = 1, \dots, N$) under the constraint $\sum_\alpha |X_{i_c, \alpha}|^2 = N$. It is known that the $N \rightarrow \infty$ model is solvable for no quantum fluctuations, so the O(2) model underestimating quantum fluctuations is used to understand the Mott transition qualitatively.

We construct the Lagrangian in the slave-rotor representation, in which there are Lagrange multipliers h and λ for the constraints. The angular momentum field L as a conjugate field will be integrated out as we do the replacement $L \rightarrow \partial_\tau \theta / U$ in some way. To treat the H_t term, we repeat the mean field procedure decoupling the spinon and rotor $H_t \rightarrow H_{t,X}^{\text{MF}} + H_{t,f}^{\text{MF}}$, by contracting all possible correlation functions $\mathcal{Z}_{i_c j_c} \equiv \langle X_{i_c}^* X_{j_c} \rangle - Z$ and χ_{ij}^κ based on the Hartree-Fock principle. This is based on the assumption that we neglect its dynamical fluctuations. Finally, we have the Lagrangians of the rotor and the spinon, and hence Green's functions $G_X(i\nu_n, \mathbf{q})$ and $G_f^\kappa(i\omega_n, \mathbf{k})$. Owing to their lengthy formulae, we show the details in Appendix C.

In the mean-field viewpoint, the correlation functions as well as the Lagrange multipliers in the Green's functions take saddle-point values. To have that, these

Green's functions must satisfy the equations

$$\langle |X_{ic}|^2 \rangle = \frac{1}{\beta N_c} \sum_{\nu_n, \mathbf{q}} G_X(i\nu_n, \mathbf{q}) = 1, \quad (12)$$

$$\langle X_{ic}^* X_{jc} \rangle = \frac{1}{\beta N_c} \sum_{\nu_n, \mathbf{q}} e^{-i\mathbf{q}(\mathbf{r}_i - \mathbf{r}_j)} G_X(i\nu_n, \mathbf{q}) = Z + \mathcal{Z}_{icjc}, \quad (13)$$

$$\langle f_{\kappa i \sigma}^\dagger f_{\kappa i \sigma} \rangle = \frac{1}{\beta N_c} \sum_{\omega_n, \mathbf{k}} e^{i\omega_n 0^+} G_f^\kappa(i\omega_n, \mathbf{k}) = \frac{1}{4} \left(1 - \frac{x}{2}\right), \quad (14)$$

$$\langle f_{\kappa i \sigma}^\dagger f_{\kappa j \sigma} \rangle = \frac{1}{\beta N_c} \sum_{\omega_n, \mathbf{k}} e^{-i\mathbf{k}(\mathbf{r}_i - \mathbf{r}_j)} G_f^\kappa(i\omega_n, \mathbf{k}) = \chi_{ij}^\kappa, \quad (15)$$

which correspond to self-consistent equations for the parameters.

We show the results in Fig. 3 by Z (NLS), Z_{BW} (NLS), and Δ_{charge} (NLS). Both the quasiparticle weight Z and the bandwidth renormalization Z_{BW} dwindle with U but differently because of the introduction of \mathcal{Z}_{icjc} and also the nonlinear band renormalization by $Z + \mathcal{Z}_{icjc}$. In the Mott insulator phase $U > U_c \approx 1.96$ meV, $Z = 0$ while Z_{BW} remains finite. The latter, which is close to Z_1 in the two-site approximation, is quite small; for example, $Z_{\text{BW}} \approx 0.12, 0.06$ and 0.03 at $U = 2, 3$ and 5 meV, respectively. Another important quantity is the excitation gap of the rotor Δ_{charge} , attributed to the Mott gap, appearing and growing quite linearly with U in the Mott insulator phase. Physically, when the rotor has a gapless spectrum with the minimum at $\mathbf{q} = \mathbf{0}$, it tends to condensate at low temperatures. Contrarily, a gapful system will forbid the condensation and exhibit short-range correlations. Notably, compared present result with previous results, U_c is further suppressed. Now U_c is quite closed to $6t_1 \approx 1.99$ meV, a bandwidth of only 1NN hopping, inferring that the system is more "flat" than band theory calculations.

IV. ANTIFERROMAGNETISM AND SUPERCONDUCTIVITY

After the study of the Mott physics at $x = 0$, we investigate antiferromagnetic (AFM) and superconducting (SC) instabilities in the cluster Hubbard model. We will demonstrate that the pair attraction arises naturally through spin/valley fluctuations in this strongly-correlated and highly-degenerate system.

Our interest is in the strong-correlation regime, so we uncover the instabilities from the large U/t side. In the large U/t limit, an effective interaction for the low-energy states, from second order perturbation, emerges as

$$H_J = -\frac{1}{2U} \mathcal{P} H_t \mathcal{Q} H_t \mathcal{P}, \quad (16)$$

where \mathcal{P} is the projection operator to a space of the least cluster interaction energy, that is $N_c(1 - |x|)$ hexagons

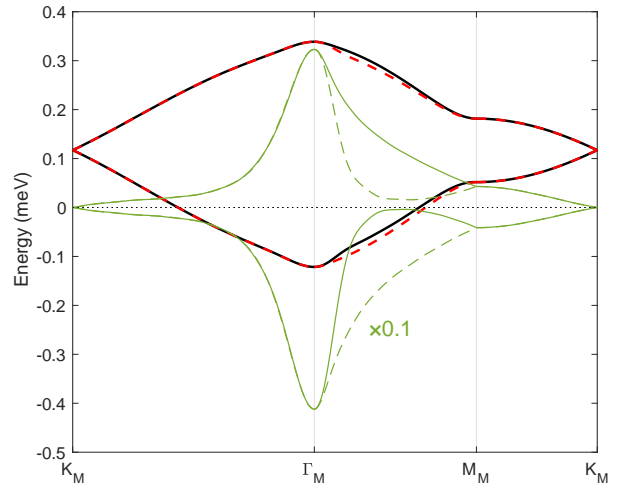


FIG. 4. Band structures for the renormalization factor $Z = 0.205$ (thick black and red lines) and $Z = 1$ (thin green lines). The solid and dashed lines represent bands at two valleys K and K' , respectively. The renormalized bands are based on the single-site approximation at U and $x = -0.06$. The bare bands ($Z = 1$) are scaled by $1/10$ to allow for better comparison. The hopping parameters, adopted from Ref.³¹, included are up to distance $r < 9a$.

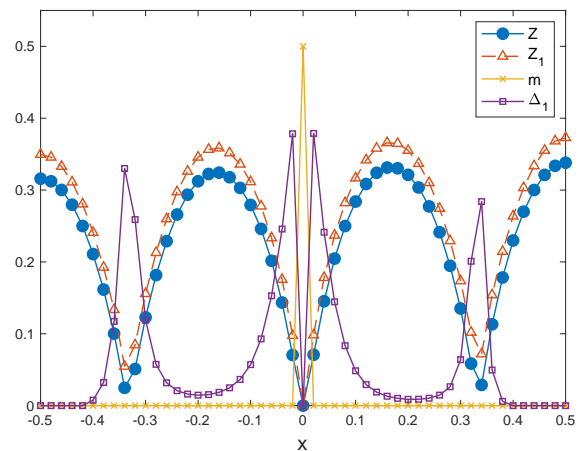


FIG. 5. Mean-field phase diagram based on the band structure in the two-site approximation at $U = 5$ meV and $J_0 = 0.2$ meV. Mott insulator phases for $Z = 0$ appear at $x = 0, \pm \frac{1}{3}$.

with six particles and $N_c|x|$ hexagons with five particles for hole doping ($x > 0$) or seven particles for electron doping ($x < 0$). (N_c is the number of the moiré unit cell and $|x|$ is the doping concentration.) Accordingly, \mathcal{Q} projects into a space of the minimal interaction energy suffered after hopping, which suggests that the virtual hopping process happens only among hexagons of six

charges. Considering the statistical counting and 1NN hopping contribution only ($t_1 \in \mathbb{R}$), we approximate

$$H_J \approx -J \sum_{\langle ij \rangle} \sum_{\kappa, \kappa'} \sum_{\sigma, \sigma'} c_{\kappa i \sigma}^\dagger c_{\kappa j \sigma} c_{\kappa' j \sigma'}^\dagger c_{\kappa' i \sigma'}, \quad (17)$$

where $\langle ij \rangle$ are NN sites and the doping-dependent coupling is $J = (1 - |x|)^2 J_0$. The coupling constant J_0 will be regarded as an independent parameter instead of t_1^2/U later.

Since H_J does not create rotor excitations but agitates spinon movement, the spinon operator f^\dagger can take over c^\dagger there. The mean-field form of H_J writes

$$H_J^{\text{MF}} = -J \sum_{\mathbf{k}} \sum_{\kappa, \sigma} \left\{ \sigma \frac{1}{2} \Delta \sum_l e^{i\mathbf{k} \cdot \mathbf{d}_l} f_{\kappa A \mathbf{k} \sigma}^\dagger f_{\kappa B - \mathbf{k} \sigma}^\dagger + \text{H.c.} \right. \\ \left. + \sigma \kappa \frac{3}{2} m \left(f_{\kappa A \mathbf{k} \sigma}^\dagger f_{\kappa A \mathbf{k} \sigma} - f_{\kappa B \mathbf{k} \sigma}^\dagger f_{\kappa B \mathbf{k} \sigma} \right) \right\}, \quad (18)$$

where two possible orders are introduced: the AFM order $m_\kappa = \pm \sum_\sigma \sigma \langle n_{\kappa i \sigma} \rangle$ and the SC pairing $\Delta^{(l)} = \sum_\sigma \sigma \langle f_{\kappa B i + \mathbf{d}_l \bar{\sigma}} f_{\kappa A i \sigma} \rangle$. The AFM order is formed between electrons at the same valley, and $m_+ = -m_- = m$ will be taken to reflect inversion symmetry. The SC pairing is formed between electrons at opposite valleys, giving zero net momentum. The most stable solution we found in the interested region is of s -wave (rotationally invariant), $\Delta^{(l)} = \Delta_s$, spin-singlet and valley-symmetric. Our solution gives a uniform system without additional periods. The model does not show the inter-valley coherence wave³⁰ too because of no feature of Fermi surface nesting in the band structure²⁴. We remark that we do not extract the Hartree-Fock self-energy in H_J to avoid double counting of interaction since H_J originates from H_U . The self-energy has been considered in spatial correlations.

We added H_J^{MF} to H' and solved the model at zero temperature using the two-site approximation for the rotor section. The phase diagram at $U = 5$ meV and $J_0 = 0.2$ meV within the doping range $|x| \leq 0.5$ is shown in Fig. 5. Repeating dome-shaped Z and Z_1 are present and they reach minima at $x = 0, \pm \frac{1}{3}, \pm \frac{2}{3}, \dots$, which correspond to the hexagon charge $Q = 6, 6 \pm 1, 6 \pm 2, \dots$, respectively. At these doping concentrations, $Z = 0$ for the choice of $U = 5$ meV greater than U_c , featuring Mott insulation. The spatial correlation Z_1 gives us a sense of the bandwidth about $Z_1 \times 1.99$ meV. It would be a defect of the theory that Z_1 , supposed to be finite, drops to zero at $x = 0$ in the presence of the AFM order.

The AFM order appears at $x = 0$ and is destroyed exceedingly fast with doping. From the linear gap equation at T_c , the critical value of J for the AFM instability is of order of the Fermi energy, and that explains the quick suppression as Fig. 5 shows. As for SC pairing, it appears for the effective attraction respecting the BCS theory and shows humps centered at Mott insulator phases where the attraction is comparatively strong. We found that the spin-singlet valley-symmetric s -wave pairing is the

most stable solution in our interesting parameter region. Since the pairing of spinons in the Mott insulator phases does not indicate superconductivity because of absence of coherence¹⁴, the result infers that superconductivity is observed noticeably proximity to the Mott insulator phases.

V. KEKULÉ VALENCE BOND ORDER

Lastly, we investigate the instability of the lattice. In this theory, we did not observe a tendency of the inter-valley coherence wave or a C_3 -symmetry breaking^{24,30}. Instead, a KVB is a possible tendency as proposed by Xu *et al.*²⁷. A direct hint of the instability is due to the observation of an unpleasant rotor dispersion. In our simulation in Sec. III C, we found that in the Mott phase, there is no rotor spatial correlations except $Z_1 \equiv Z_1 - Z$, indicating that rotors hop on a triangular lattice (more correctly, on three independent lattices) with distance $\sqrt{3}a = |\mathbf{a}'_1|$. In consequence, the rotor is energetically degenerate at Γ and three K points according to the dispersion $\varepsilon_X(\mathbf{q}) \propto \sum_l \cos(\mathbf{q} \cdot \mathbf{a}'_l)$. The degeneracy is not stable and should be lift once Bose condensation occurs. As a result, an order with wave vector $\mathbf{K} = \frac{2\pi}{3a}(\sqrt{3}\hat{x} + \hat{y})$ might emerge.

Based on this argument, we assume a KVB in the spinon section as

$$\sum_\sigma \left\langle f_{\kappa A i \sigma}^\dagger f_{\kappa B i + \mathbf{d}_i \sigma} \right\rangle = \chi_1 + \chi'_1 \cos[\mathbf{K} \cdot (\mathbf{r}_i - \mathbf{d}_i)]. \quad (19)$$

The order is shown in Fig. 5 where thick and thin lines indicate strong bonds $\chi_+ = \chi_1 + \chi'_1$ and weak bonds $\chi_- = \chi_1 - \frac{1}{2}\chi'_1$, respectively. The KVB preserves the C_3 symmetry and has a threefold enlarged unit cell containing three hexagons labelled by 1, 2, and 3 in Fig. 5. The modulation in the spinon section will induce the order in the rotor section as well. We define the rotor's condensate fraction $\langle e^{i\theta_{ic}} \rangle$ as $\sqrt{Z_+}$ at site 1 and as $\sqrt{Z_-}$ at site 2 and 3, respectively. Similarly, the rotor correlation $\langle e^{i\theta_{ic}} e^{-i\theta_{jc}} \rangle$ as Z_{1+} for $(i_c, j_c) = (1, 1')$ and Z_{1-} for $(i_c, j_c) = (2, 2')$ and $(3, 3')$.

With this assumption, we repeat the self-consistent calculation using the two-site approximation. Due to computational limit, in this section, we neglect long-range hopping except the 1NN hopping (t_1), or a much larger cluster for the correlation is needed. Meanwhile, on top of the KVB, we investigate AFM and SC instabilities from H_J in Eq. (17). The AFM order is defined as before in Sec. IV, while the SC order is $\sum_\sigma \sigma \langle f_{\kappa B i + \mathbf{d}_i \bar{\sigma}} f_{\kappa A i \sigma} \rangle = \Delta_s + \Delta'_s \cos[\mathbf{K} \cdot (\mathbf{r}_i - \mathbf{d}_i)]$. (The s wave is still stronger than the $d + id$ wave.)

The phase diagram as doping at $U = 5$ meV and $J_0 = 0.2$ meV is shown in Fig. 7, in which we find the KVB occurs around the fractional doping $x = 0, \pm \frac{1}{3}$, where $Z_+ \neq Z_-$. The SC order shows strong modulation $\Delta'_s > \Delta_s$ on top of the KVB order, and the AFM order is unfavorable completely. Remarkably, the condensate

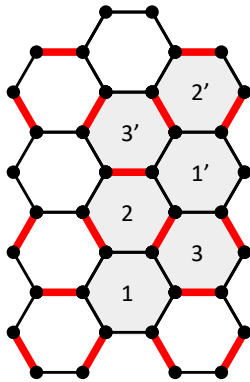


FIG. 6. Kekulé valence bond order as a modulation of hopping amplitudes with strong NN bonds (red thick lines) and weak NN bonds (black thin lines). The order enlarges the unit cell containing three hexagons labelled by 1, 2, and 3. Three pairs of hexagons [(1,1'), (2,2'), and (3,3')] are considered to study rotor correlation.

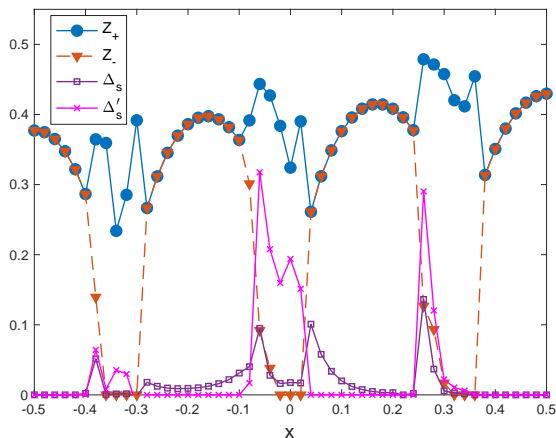


FIG. 7. Phase diagram of the Kekulé valence bond order as well as s -wave superconductivity at $U = 5$ meV and $J_0 = 0.2$ meV when only the 1NN hopping is considered. When $Z_+ \neq Z_-$ or $\Delta'_s \neq 0$, the Kekulé valence bond order is present.

fraction Z_- is zero for a finite doping range nearby the fractional doping, whereas Z_+ is finite. At these doping concentrations, the system is an insulator phase, named a Kekulé valence bond solid, because charge is localized at hexagons 2 and 3 and cannot propagate. As a result, the KVB will extend the Mott insulator phase, giving us a phase diagram quite similar to what experiments observed^{1,2}. Whether the KVB is the origin of the correlated phase awaits future investigation.

VI. CONCLUSIONS

In this work, we have applied the slave-rotor theory on the cluster Hubbard model based on the peculiar Wannier orbitals of magic-angle TBG. The slave-rotor will play the role of the charge degree of freedom in a hexagon (six sites). Due to strong correlation, charge fluctuation is suppressed to exhibit Mott physics. More than what suggested^{10,12,26,39}, the theory predicts multiple Mott insulator phases at fractional filling with $n = 2$ (two charges per moiré unit cell), $2 \pm \frac{1}{3}$, $2 \pm \frac{2}{3}$, 2 ± 1 etc. In addition, the theory suggests a Kekulé valence bond solid phase Xu *et al.*²⁷ nearby the fractional filling. Experimental results from scanning tunnelling microscopy showed prominent depression of spectrum at $n = 2$ and weaker ones $n = 1$ and 3 ^{1,9,10,12,13}; However, exotic dips seemed present in between, which awaits attentive examination; similar features were seen in transport measurements¹³. With doping away from the Mott insulator, due to spin-valley fluctuations s -wave superconductivity emerges naturally by breaking approximate $SO(4)$ symmetry²⁴. Lastly, we comment that our slave-rotor theory for the system does not enumerate cluster states which have discriminative roles in hopping⁴⁰. Many nontrivial phases^{13,41} might be due to the nonlocal cluster interaction, and advanced techniques for cluster theories will be required⁴²⁻⁴⁴. Nevertheless, our theory incorporating Mott physics provides an important ground for the highly correlated and degenerate system.

ACKNOWLEDGMENTS

S.M.H and T.K.L thank F. Yang for helpful discussions. S.M.H. is supported by the Ministry of Science and Technology (MoST) in Taiwan under Grant No.105-2112-M-110-014-MY3 and No. 108-2112-M-110-013-MY3. Y.-P.H receives funding from the European Union's Horizon 2020 research and innovation program under the Marie Skłodowska-Curie grant agreement No. 701647.

Appendix A: Local gauge symmetry

We demonstrate the local gauge symmetry present in this slave-rotor theory. In a typical slave-particle theory, taking the slave-boson theory for example¹⁴, an electron operator c is written as a product of a boson b and a fermion operator f : $c_i^\dagger = b_i f_i^\dagger$. Because both f and b locate at the same site i , one can understand a local gauge symmetry in the theory that under the local gauge transformation

$$f_i^\dagger \rightarrow e^{i\phi_i} f_i^\dagger, \quad b_i \rightarrow e^{-i\phi_i} b_i$$

the system is invariant. The local gauge symmetry implies particle conservation that the net current of f and b particles is zero: $j_f^\mu + j_b^\mu = 0$ and an internal gauge

field a_μ couples to f and b particles simultaneously (μ for spacetime labels)¹⁴.

In our slave-rotor theory, a rotor stands for the charge in a hexagon which shares with many spinons at the corner, so that it is impossible to find a gauge-invariant transformation just on a rotor and a spinon. Differently, we will show the local gauge transformation is on the spinon and rotor dipoles. The existence of a local gauge symmetry is because we can find that a hop of an electron as well as a spinon always accompanies with a hop of a rotor (hexagon charge), an indication of charge conservation. Besides, according to the definition in Eq. (4), an electron creation operator takes three rotor raising operators, so a phase operator $e^{i\theta}$ create a charge of $1/3$.

Let's discuss the transformations one by one. Firstly, refer to Fig. 2(a). It describes a NN hopping as $c_{\mathbf{r}_i}^\dagger c_{\mathbf{r}_i+\mathbf{d}_l}$ (with $l = 1$), which becomes $f_{\mathbf{r}_i}^\dagger f_{\mathbf{r}_i+\mathbf{d}_l} X_{\mathbf{r}_i-\mathbf{d}_l}^* X_{\mathbf{r}_i+2\mathbf{d}_l}$ after substitution, where we omit the spin-valley index and use $X_{i_c}^* \equiv e^{i\theta_{i_c}}$. The four-operator term possesses a local gauge symmetry under the transformation:

$$f_{\mathbf{r}_i}^\dagger f_{\mathbf{r}_i+\mathbf{d}_l} \rightarrow e^{i\phi_{\mathbf{r}_i+\frac{1}{2}\mathbf{d}_l}} f_{\mathbf{r}_i}^\dagger f_{\mathbf{r}_i+\mathbf{d}_l}, \quad (\text{A1})$$

$$X_{\mathbf{r}_i-\mathbf{d}_l}^* X_{\mathbf{r}_i+2\mathbf{d}_l} \rightarrow e^{-i\phi_{\mathbf{r}_i+\frac{1}{2}\mathbf{d}_l}} X_{\mathbf{r}_i-\mathbf{d}_l}^* X_{\mathbf{r}_i+2\mathbf{d}_l}, \quad (\text{A2})$$

where the gauge phase is define at the center of the NN bond $\mathbf{r}_i + \frac{1}{2}\mathbf{d}_l$. We can interpret the above equations as a gauge transformation on a spinon and a rotor dipole. The rotor dipole and its transformation will be an elementary one as seen later. As the rotor dipole is three-fold the length of that of the spinon dipole, the rotor's velocity is three times as big as the spinon's in this hopping, agreeing with equal currents of the spinon and the rotor.

Next, we consider the gauge transformation in Fig. 2(b), where we can find a spinon dipole of length a and two rotor dipoles of length $3|\mathbf{d}_l|$. To make consistent with before, if the rotor dipoles transform according to Eq. (A2), the spinon dipole of length a has to transform as

$$f_{\mathbf{r}_i}^\dagger f_{\mathbf{r}_i-\mathbf{a}_l} \rightarrow e^{i\phi_{\mathbf{r}_i-\frac{1}{2}\mathbf{a}_{l+1}}} e^{i\phi_{\mathbf{r}_i-\mathbf{a}_{l+1}+\frac{1}{2}\mathbf{a}_{l-1}}} f_{\mathbf{r}_i}^\dagger f_{\mathbf{r}_i-\mathbf{a}_l}, \quad (\text{A3})$$

(with $l = 2$) where the gauge phase connecting \mathbf{r}_i and $\mathbf{r}_i - \mathbf{a}_l$ is defined as an addition of a gauge phase at two bond centers $\mathbf{r}_i - \frac{1}{2}\mathbf{a}_{l+1}$ and $\mathbf{a}_{l+1} + \frac{1}{2}\mathbf{a}_{l-1}$.

Lastly, we discuss the 3NN hopping case in Fig. 2(c), where $c_{\mathbf{r}_i}^\dagger c_{\mathbf{r}_i+\mathbf{D}_l}$ ($l = 1$) arises. In Fig. 2(c), there are two rotor dipoles transformed according to Eq. (A2). To make gauge invariant, the spinon dipole of length $|\mathbf{D}_l|$ should follow the transformation:

$$f_{\mathbf{r}_i}^\dagger f_{\mathbf{r}_i+\mathbf{D}_l} \rightarrow e^{i\phi_{\mathbf{r}_i+\mathbf{d}_{l+1}-\frac{1}{2}\mathbf{a}_l}} e^{i\phi_{\mathbf{r}_i+\mathbf{d}_{l-1}-\frac{1}{2}\mathbf{a}_l}} f_{\mathbf{r}_i}^\dagger f_{\mathbf{r}_i+\mathbf{D}_l}, \quad (\text{A4})$$

where the two gauge phases are conjugates of those of associated rotor dipoles. As the gauge transformations in the rest hopping terms, readers can use and combine the transformations in Eqs. (A1)-(A4).

Appendix B: Slave-rotor representation for H_t

In this Appendix, we are aim at the hopping Hamiltonian,

$$H_t = \sum_{ij} \sum_{\kappa=\pm} \sum_{\sigma=\uparrow,\downarrow} t_{ij}^\kappa c_{\kappa i \sigma}^\dagger c_{\kappa j \sigma}, \quad (\text{B1})$$

and transform physical electrons (c^\dagger) into the spinon (f^\dagger) and the slave rotor ($e^{i\theta}$) operators. We demonstrate them up to the fifth NN one. For brevity, we denote an n-th NN hopping by nNN and their corresponding hopping integrals are t_n . The honeycomb lattice shows that two sublattices A and B have different hexagon neighbors, so we define that $c_{\kappa A i \sigma}^\dagger = f_{\kappa A i \sigma}^\dagger \prod_l e^{i\theta_{i-\mathbf{d}_l}}$ and $c_{\kappa B i \sigma}^\dagger = f_{\kappa B i \sigma}^\dagger \prod_l e^{i\theta_{i+\mathbf{d}_l}}$. In this formalism, a 1NN brings out two phase factors, while 2NN and 3NN give four. As for 4NN and 5NN as well as longer-ranged hoppings, they give six phase factors.

In addition, we will decompose the spinon and the rotor by the Hatree-Fock mean field theory to have a bilinear form of the hopping Hamiltonian. The complex bosonic field $X \equiv e^{-i\theta}$ will be used. For the simplest mean-field, one is to take $\langle X \rangle = \sqrt{Z}$ for condensation of the rotor. Here we are going to consider the spatial correlations from excitations of the rotors. In the spirit of Bose condensation, we write $X = \sqrt{Z} + \delta X$, the latter for the non-condensate component. We define the correlation functions for the spinon and the rotor as

$$\chi_{\mathbf{r}}^\kappa = \sum_{\sigma} \left\langle f_{\kappa i \sigma}^\dagger f_{\kappa i+\mathbf{r} \sigma} \right\rangle, \quad (\text{B2})$$

$$\mathcal{Z}_{\mathbf{R}} = \langle \delta X_{i_c}^* \delta X_{i_c+\mathbf{R}} \rangle = \langle \delta X_{i_c} \delta X_{i_c+\mathbf{R}}^* \rangle. \quad (\text{B3})$$

Since rotors are assigned to hexagon sites, \mathbf{R} in $\mathcal{Z}_{\mathbf{R}}$ has to be a crystal translation vector, while \mathbf{r} in $\chi_{\mathbf{r}}$ depends on whether it is an inter or intra-sublattice bond. Because of spatial symmetry, we further denote some correlation functions by

$$\begin{aligned} \chi_1^\kappa &= \chi_{\mathbf{d}_l}^\kappa, \quad \chi_2^\kappa = \chi_{\pm\mathbf{a}_l}^\kappa, \quad \chi_3^\kappa = \chi_{\mathbf{D}_l}^\kappa, \\ \chi_4^\kappa &= \chi_{\mathbf{d}_l-\mathbf{a}_{l+1}}^\kappa = \chi_{\mathbf{d}_l+\mathbf{a}_{l-1}}^\kappa, \\ \chi_5^\kappa &= \chi_{\pm(\mathbf{a}_l-\mathbf{a}_{l+1})}^\kappa, \\ \mathcal{Z}_0 &= \mathcal{Z}_{\pm\mathbf{a}_l}, \quad \mathcal{Z}_1 = \mathcal{Z}_{\pm(\mathbf{a}_l-\mathbf{a}_{l+1})}, \quad \mathcal{Z}_2 = \mathcal{Z}_{\pm 2\mathbf{a}_l}, \\ \mathcal{Z}_3 &= \mathcal{Z}_{\pm(2\mathbf{a}_l-\mathbf{a}_{l+1})} = \mathcal{Z}_{\pm(\mathbf{a}_l-2\mathbf{a}_{l+1})}, \end{aligned} \quad (\text{B4})$$

where $l = 1, 2, 3$.

After tedious derivation of the mean-field contraction and also Fourier transform, we have the decoupled mean-field Hamiltonians of the spinon and the rotor $H_t^{\text{MF}} = H_{t,f}^{\text{MF}} + H_{t,X}^{\text{MF}}$ to bilinear order:

$$\begin{aligned} H_{t,f}^{\text{MF}} &= \sum_{\mathbf{k}} \sum_{\kappa,\sigma} \left\{ h_{0,\kappa}(\mathbf{k}) \left(f_{\kappa A \mathbf{k} \sigma}^\dagger f_{\kappa A \mathbf{k} \sigma} + f_{\kappa B \mathbf{k} \sigma}^\dagger f_{\kappa B \mathbf{k} \sigma} \right) \right. \\ &\quad \left. + h_{1,\kappa}(\mathbf{k}) f_{\kappa A \mathbf{k} \sigma}^\dagger f_{\kappa B \mathbf{k} \sigma} + h_{1,\kappa}^*(\mathbf{k}) f_{\kappa B \mathbf{k} \sigma}^\dagger f_{\kappa A \mathbf{k} \sigma} \right\}, \end{aligned} \quad (\text{B5})$$

and

where

$$H_{t,X}^{\text{MF}} = \sum_{\mathbf{q}} \varepsilon_X(\mathbf{q}) X_{\mathbf{q}}^* X_{\mathbf{q}}, \quad (\text{B6})$$

$$\begin{aligned} h_{0,\kappa}(\mathbf{k}) &= 2t_2^\kappa [Z^2 + Z(\mathcal{Z}_0 + 2\mathcal{Z}_1 + \mathcal{Z}_2) + \mathcal{Z}_1^2 + \mathcal{Z}_0\mathcal{Z}_2] \sum_l \cos(\mathbf{k} \cdot \mathbf{a}_l) \\ &\quad + 2t_5^\kappa [Z^3 + Z^2(2\mathcal{Z}_0 + 3\mathcal{Z}_1 + 2\mathcal{Z}_2 + 2\mathcal{Z}_3) \\ &\quad + Z(3\mathcal{Z}_1^2 + \mathcal{Z}_2^2 + 2\mathcal{Z}_0\mathcal{Z}_1 + 2\mathcal{Z}_0\mathcal{Z}_2 + 3\mathcal{Z}_0\mathcal{Z}_3 + 2\mathcal{Z}_1\mathcal{Z}_2 + 2\mathcal{Z}_1\mathcal{Z}_3 + 2\mathcal{Z}_2\mathcal{Z}_3) \\ &\quad + \mathcal{Z}_1^3 + \mathcal{Z}_1\mathcal{Z}_2^2 + 2\mathcal{Z}_0\mathcal{Z}_1\mathcal{Z}_3 + 2\mathcal{Z}_0\mathcal{Z}_2\mathcal{Z}_3] \sum_l \cos(\mathbf{k} \cdot \mathbf{a}'_l) \\ &= 2t_2^\kappa (Z + \mathcal{Z}_1)^2 \sum_l \cos(\mathbf{k} \cdot \mathbf{a}_l) + 2t_5^\kappa (Z + \mathcal{Z}_1)^3 \sum_l \cos(\mathbf{k} \cdot \mathbf{a}'_l) \end{aligned} \quad (\text{B7})$$

$$\begin{aligned} h_{1,\kappa}(\mathbf{k}) &= t_1^\kappa (Z + \mathcal{Z}_1) \sum_l e^{i\mathbf{k} \cdot \mathbf{d}_l} + t_3^\kappa [Z^2 + Z(2\mathcal{Z}_1 + 2\mathcal{Z}_2) + \mathcal{Z}_1^2 + \mathcal{Z}_2^2] \sum_l e^{i\mathbf{k} \cdot \mathbf{D}_l} \\ &\quad + t_4^\kappa [Z^3 + Z^2(3\mathcal{Z}_0 + 3\mathcal{Z}_1 + 2\mathcal{Z}_2 + \mathcal{Z}_3) \\ &\quad + Z(\mathcal{Z}_0^2 + 3\mathcal{Z}_1^2 + \mathcal{Z}_2^2 + 3\mathcal{Z}_0\mathcal{Z}_1 + 4\mathcal{Z}_0\mathcal{Z}_2 + 3\mathcal{Z}_0\mathcal{Z}_3 + 2\mathcal{Z}_1\mathcal{Z}_2 + \mathcal{Z}_1\mathcal{Z}_3) \\ &\quad + \mathcal{Z}_1^3 + \mathcal{Z}_0\mathcal{Z}_2^2 + \mathcal{Z}_0^2\mathcal{Z}_3 + 2\mathcal{Z}_1\mathcal{Z}_0\mathcal{Z}_2 + \mathcal{Z}_1\mathcal{Z}_0\mathcal{Z}_3] \sum_l e^{i\mathbf{k} \cdot \mathbf{d}_l} (e^{-i\mathbf{k} \cdot \mathbf{a}_{l+1}} + e^{i\mathbf{k} \cdot \mathbf{a}_{l-1}}) \\ &= t_1^\kappa (Z + \mathcal{Z}_1) \sum_l e^{i\mathbf{k} \cdot \mathbf{d}_l} + t_3^\kappa (Z + \mathcal{Z}_1)^2 \sum_l e^{i\mathbf{k} \cdot \mathbf{D}_l} + t_4^\kappa (Z + \mathcal{Z}_1)^3 \sum_l e^{i\mathbf{k} \cdot \mathbf{d}_l} (e^{-i\mathbf{k} \cdot \mathbf{a}_{l+1}} + e^{i\mathbf{k} \cdot \mathbf{a}_{l-1}}) \end{aligned} \quad (\text{B8})$$

and

$$\begin{aligned} \varepsilon_X(\mathbf{q}) &= \{2(Z + \mathcal{Z}_2)K_2 + 2[3Z^2 + Z(2\mathcal{Z}_0 + 3\mathcal{Z}_1 + 3\mathcal{Z}_2 + 3\mathcal{Z}_3) + 2\mathcal{Z}_1\mathcal{Z}_2 + \mathcal{Z}_1\mathcal{Z}_3 + 2\mathcal{Z}_0\mathcal{Z}_3 + \mathcal{Z}_2^2] K_4 \\ &\quad + 4[Z^2 + Z(\mathcal{Z}_1 + \mathcal{Z}_2 + 2\mathcal{Z}_3) + \mathcal{Z}_1\mathcal{Z}_3 + \mathcal{Z}_2\mathcal{Z}_3] K_5\} \sum_l \cos(\mathbf{q} \cdot \mathbf{a}_l) \\ &\quad + \{K_1 + 4(Z + \mathcal{Z}_1)K_2 + 2(Z + \mathcal{Z}_1)K_3 \\ &\quad + 2[3Z^2 + Z(3\mathcal{Z}_0 + 6\mathcal{Z}_1 + 2\mathcal{Z}_2 + \mathcal{Z}_3) + 3\mathcal{Z}_1^2 + 2\mathcal{Z}_0\mathcal{Z}_2 + \mathcal{Z}_1\mathcal{Z}_3] K_4 \\ &\quad + 2[3Z^2 + Z(2\mathcal{Z}_0 + 6\mathcal{Z}_1 + 2\mathcal{Z}_2 + 2\mathcal{Z}_3) + 3\mathcal{Z}_1^2 + \mathcal{Z}_2^2 + 2\mathcal{Z}_0\mathcal{Z}_3] K_5\} \sum_l \cos(\mathbf{q} \cdot \mathbf{a}'_l) \\ &\quad + \{2(Z + \mathcal{Z}_0)K_2 + 2(Z + \mathcal{Z}_2)K_3 \\ &\quad + 4[Z^2 + Z(2\mathcal{Z}_0 + \mathcal{Z}_1 + \mathcal{Z}_2) + \mathcal{Z}_0\mathcal{Z}_2 + \mathcal{Z}_1\mathcal{Z}_0] K_4 \\ &\quad + 4[Z^2 + Z(\mathcal{Z}_0 + \mathcal{Z}_1 + \mathcal{Z}_2 + \mathcal{Z}_3) + \mathcal{Z}_1\mathcal{Z}_2 + \mathcal{Z}_0\mathcal{Z}_3] K_5\} \sum_l \cos(\mathbf{q} \cdot 2\mathbf{a}_l) \\ &\quad + \{[Z^2 + Z(3\mathcal{Z}_0 + \mathcal{Z}_1) + \mathcal{Z}_0^2 + \mathcal{Z}_0\mathcal{Z}_1] K_4 \\ &\quad + 2[Z^2 + Z(2\mathcal{Z}_0 + \mathcal{Z}_1 + \mathcal{Z}_2) + \mathcal{Z}_0\mathcal{Z}_1 + \mathcal{Z}_0\mathcal{Z}_2] K_5\} \sum_l (\cos[\mathbf{q} \cdot (2\mathbf{a}_l - \mathbf{a}_{l+1})] + \cos[\mathbf{q} \cdot (\mathbf{a}_l - 2\mathbf{a}_{l+1})]) \\ &= 2Z[K_2 + (Z + \mathcal{Z}_1)(3K_4 + 2K_5)] \sum_l \cos(\mathbf{q} \cdot \mathbf{a}_l) \\ &\quad + [K_1 + (Z + \mathcal{Z}_1)(4K_2 + 2K_3) + 6(Z + \mathcal{Z}_1)^2(K_4 + K_5)] \sum_l \cos(\mathbf{q} \cdot \mathbf{a}'_l) \\ &\quad + 2Z[K_2 + K_3 + 2(Z + \mathcal{Z}_1)(K_4 + K_5)] \sum_l \cos(\mathbf{q} \cdot 2\mathbf{a}_l) \\ &\quad + Z(Z + \mathcal{Z}_1)(K_4 + 2K_5) \sum_l (\cos[\mathbf{q} \cdot (2\mathbf{a}_l - \mathbf{a}_{l+1})] + \cos[\mathbf{q} \cdot (\mathbf{a}_l - 2\mathbf{a}_{l+1})]) \end{aligned} \quad (\text{B9})$$

with

$$K_{i=1,2,3,4,5} = \sum_{\kappa} t_i^\kappa \chi_i^\kappa + \text{c.c.} = 4 \text{Re}(t_i^\kappa \chi_i^\kappa). \quad (\text{B10})$$

The last lines of Eqs. (B7-B9) show the results when

$\mathcal{Z}_0 = \mathcal{Z}_2 = \mathcal{Z}_3 = 0$. The above formulae, for brevity, omit the rotor's anomalous correlation $\langle \delta X_{i_c} \delta X_{i_c + \mathbf{a}_i} \rangle$, which might emerge when $Z \neq 0$, for its make the formulae much lengthy but its smallness is actually ineffective.

We note that our simulation results showed $\mathcal{Z}_0 = \mathcal{Z}_2 = \mathcal{Z}_3 = 0$ and only \mathcal{Z}_1 being finite in the Mott insulator phase ($Z = 0$). The result is reasonable because the former order parameters do not appear linearly in H_t^{MF} and H_X^{MF} ; solutions of this type system are zeros commonly and become finite through a discontinuous first-order phase transition when some couplings are greater than critical values.

Appendix C: Action in slave-rotor representation

The action of the system in terms of the rotor and the spinon particles will be demonstrated. The Hatree-Fock mean field theory will be adopted to deal with the hopping Hamiltonian H_t . The adoption of the mean field theory leads to several self-consistent equations, which will be shown here as well. Since the presentation here is aimed at the Mott transition, it will not include anti-ferromagnetism and superconductivity.

The imaginary-time action reads

$$S = \int_0^\beta d\tau \left\{ -i \sum_{i_c} L_{i_c} \partial_\tau \theta_{i_c} + \sum_{i, \kappa, \sigma} \bar{f}_{\kappa i \sigma} \partial_\tau f_{\kappa i \sigma} + H_t + U \sum_{i_c} L_{i_c}^2 + h \sum_{i_c} \left(L_{i_c} - \sum_{i \in i_c} \bar{f}_{\kappa i \sigma} f_{\kappa i \sigma} + 6 \right) \right\}, \quad (\text{C1})$$

where i and i_c run over sublattice and hexagon sites, respectively. The hopping Hamiltonian H_t , not shown explicitly here, is referred to Appendix B. The conjugate field angular momentum L_{i_c} will be integrated out to

change to $\partial_\tau \theta_{i_c}$, giving

$$S = \int_0^\beta d\tau \left\{ \sum_{i, \kappa, \sigma} \bar{f}_{\kappa i \sigma} (\partial_\tau - 3h) f_{\kappa i \sigma} + H_t + \frac{1}{4U} \sum_{i_c} (\partial_\tau \theta_{i_c} + ih)^2 + 6hN_c \right\}. \quad (\text{C2})$$

Now, we will replace $e^{-i\theta_{i_c}}$ by X_{i_c} with the constraint $|X_{i_c}|^2 = 1$, which is realized with the aid of the Lagrange multiplier λ . Meanwhile, we have to scale U to $\frac{U}{2}$, as pointed out in Refs.^{36,37}, in order to have consistent connection with the large- M limit of the $O(2M)$ model. (We admit this is a bold assumption because this is based on the atomic limit and cannot explain full spectrum^{36,37}.) Therefore, the action becomes

$$S = \int_0^\beta d\tau \left\{ \sum_{i, \kappa, \sigma} \bar{f}_{\kappa i \sigma} (\partial_\tau - 3h) f_{\kappa i \sigma} + H_t + \sum_{i_c} \left[\frac{1}{2U} |\partial_\tau X_{i_c}|^2 + \frac{h}{2U} (X_{i_c} \partial_\tau X_{i_c}^* - \text{H.c.}) + \lambda |X_{i_c}|^2 \right] \right\} + \beta N_c \left(6h - \frac{h^2}{2U} - \lambda \right). \quad (\text{C3})$$

Although the Lagrange multipliers h and λ are variables to be integrated out, they are treated as constants of their saddle-point values in practice. With the assumption, Green's functions of the spinon and the rotor are obtained. The self-energies of the spinon and the rotor come from H_t that describes the coupling between them. To make it simple, we simply substitute $H_t^{\text{MF}} = H_{t,f}^{\text{MF}} + H_{t,X}^{\text{MF}}$ (see it in Appendix B) for H_t in S , which implies that dynamical fluctuations from H_t are omitted. The Green's functions are, therefore,

$$G_f^\kappa(i\omega_n, \mathbf{k}) = \left[i\omega_n - \begin{pmatrix} h_{0,\kappa}(\mathbf{k}) & h_{1,\kappa}(\mathbf{k}) \\ h_{1,\kappa}^*(\mathbf{k}) & h_{0,\kappa}(\mathbf{k}) \end{pmatrix} \right]^{-1}, \quad (\text{C4})$$

$$G_X(i\nu_n, \mathbf{q}) = Z\beta \delta_{n,0} \delta(\mathbf{q}) - \frac{2U}{(i\nu_n + h)^2 - 2U[\varepsilon_X(\mathbf{q}) + \lambda]}, \quad (\text{C5})$$

where we have absorbed $3h$ into μ in G_f and $\frac{h^2}{2U}$ into λ in G_X . In order to have a stable rotor system, $\varepsilon_X(\mathbf{q}) + \lambda \geq 0$ for all \mathbf{q} . So we rewrite $\varepsilon_X(\mathbf{q}) + \lambda$ to be $[\varepsilon_X(\mathbf{q}) - \varepsilon_X(\mathbf{0})] + \Delta_{\text{charge}}^2/2U$, where Δ_{charge} stands for the Mott gap. All the parameters Z , Δ_{charge} , μ , and correlation functions are determined self-consistently from Eqs. (12)-(15).

¹ Y. Cao, V. Fatemi, S. Fang, K. Watanabe, T. Taniguchi, E. Kaxiras, and P. Jarillo-Herrero, Nature **556**, 43 (2018).

² Y. Cao, V. Fatemi, A. Demir, S. Fang, S. L. Tomarken, J. Y. Luo, J. D. Sanchez-Yamagishi, K. Watanabe,

- T. Taniguchi, E. Kaxiras, *et al.*, *Nature* **556**, 80 (2018).
- ³ A. K. Geim and I. V. Grigorieva, *Nature* **499**, 419 (2013).
 - ⁴ R. Bistritzer and A. H. MacDonald, *Proceedings of the National Academy of Sciences* **108**, 12233 (2011).
 - ⁵ J. L. Dos Santos, N. Peres, and A. C. Neto, *Phys. Rev. Lett.* **99**, 256802 (2007).
 - ⁶ S. Shallcross, S. Sharma, E. Kandelaki, and O. Pankratov, *Phys. Rev. B* **81**, 165105 (2010).
 - ⁷ G. Trambly de Laissardière, D. Mayou, and L. Magaud, *Phys. Rev. B* **86**, 125413 (2012).
 - ⁸ G. Tarnopolsky, A. J. Kruchkov, and A. Vishwanath, *Phys. Rev. Lett.* **122**, 106405 (2019).
 - ⁹ Y. Xie, B. Lian, B. Jäck, X. Liu, C.-L. Chiu, K. Watanabe, T. Taniguchi, B. A. Bernevig, and A. Yazdani, *Nature* **572**, 101 (2019).
 - ¹⁰ Y. Choi, J. Kemmer, Y. Peng, A. Thomson, H. Arora, R. Polski, Y. Zhang, H. Ren, J. Alicea, G. Refael, *et al.*, *Nature Physics* **15**, 1174 (2019).
 - ¹¹ A. Kerelsky, L. J. McGilly, D. M. Kennes, L. Xian, M. Yankowitz, S. Chen, K. Watanabe, T. Taniguchi, J. Hone, C. Dean, *et al.*, *Nature* **572**, 95 (2019).
 - ¹² H. Polshyn, M. Yankowitz, S. Chen, Y. Zhang, K. Watanabe, T. Taniguchi, C. R. Dean, and A. F. Young, *Nature Physics* **15**, 1011 (2019).
 - ¹³ X. Lu, P. Stepanov, W. Yang, M. Xie, M. A. Aamir, I. Das, C. Urgell, K. Watanabe, T. Taniguchi, G. Zhang, A. Bachtold, A. H. MacDonald, and D. K. Efetov, *Nature* **574**, 653 (2019).
 - ¹⁴ P. A. Lee, N. Nagaosa, and X.-G. Wen, *Rev. Mod. Phys.* **78**, 17 (2006).
 - ¹⁵ H. Guo, X. Zhu, S. Feng, and R. T. Scalettar, *Phys. Rev. B* **97**, 235453 (2018).
 - ¹⁶ A. Thomson, S. Chatterjee, S. Sachdev, and M. S. Scheurer, *Phys. Rev. B* **98**, 075109 (2018).
 - ¹⁷ T. J. Peltonen, R. Ojajarvi, and T. T. Heikkilä, *Phys. Rev. B* **98**, 220504 (2018).
 - ¹⁸ C.-C. Liu, L.-D. Zhang, W.-Q. Chen, and F. Yang, *Phys. Rev. Lett.* **121**, 217001 (2018).
 - ¹⁹ J. Gonzalez and T. Stauber, *Phys. Rev. Lett.* **122**, 026801 (2019).
 - ²⁰ Q.-K. Tang, L. Yang, D. Wang, F.-C. Zhang, and Q.-H. Wang, *Phys. Rev. B* **99**, 094521 (2019).
 - ²¹ B. Roy and V. Juričić, *Phys. Rev. B* **99**, 121407 (2019).
 - ²² S. Ray, J. Jung, and T. Das, *Phys. Rev. B* **99**, 134515 (2019).
 - ²³ B. Lian, Z. Wang, and B. A. Bernevig, *Phys. Rev. Lett.* **122**, 257002 (2019).
 - ²⁴ Y.-Z. You and A. Vishwanath, *npj Quantum Materials* **4**, 16 (2019).
 - ²⁵ J. F. Dodaro, S. A. Kivelson, Y. Schattner, X.-Q. Sun, and C. Wang, *Phys. Rev. B* **98**, 075154 (2018).
 - ²⁶ M. Ochi, M. Koshino, and K. Kuroki, *Phys. Rev. B* **98**, 081102 (2018).
 - ²⁷ X. Y. Xu, K. Law, and P. A. Lee, *Phys. Rev. B* **98**, 121406 (2018).
 - ²⁸ D. M. Kennes, J. Lischner, and C. Karrasch, *Phys. Rev. B* **98**, 241407 (2018).
 - ²⁹ L. Classen, C. Honerkamp, and M. M. Scherer, *Phys. Rev. B* **99**, 195120 (2019).
 - ³⁰ H. C. Po, L. Zou, A. Vishwanath, and T. Senthil, *Phys. Rev. X* **8**, 031089 (2018).
 - ³¹ M. Koshino, N. F. Yuan, T. Koretsune, M. Ochi, K. Kuroki, and L. Fu, *Phys. Rev. X* **8**, 031087 (2018).
 - ³² D. Pesin and L. Balents, *Nature Physics* **6**, 376 (2010).
 - ³³ W.-H. Ko and P. A. Lee, *Phys. Rev. B* **83**, 134515 (2011).
 - ³⁴ C. Chamon, *Phys. Rev. B* **62**, 2806 (2000).
 - ³⁵ J. Kang and O. Vafek, *Phys. Rev. X* **8**, 031088 (2018).
 - ³⁶ S. Florens and A. Georges, *Phys. Rev. B* **66**, 165111 (2002).
 - ³⁷ S. Florens and A. Georges, *Phys. Rev. B* **70**, 035114 (2004).
 - ³⁸ E. Zhao and A. Paramekanti, *Phys. Rev. B* **76**, 195101 (2007).
 - ³⁹ M. Xie and A. H. MacDonald, *arXiv preprint arXiv:1812.04213* (2018).
 - ⁴⁰ J. Büinemann, W. Weber, and F. Gebhard, *Phys. Rev. B* **57**, 6896 (1998).
 - ⁴¹ A. L. Sharpe, E. J. Fox, A. W. Barnard, J. Finney, K. Watanabe, T. Taniguchi, M. Kastner, and D. Goldhaber-Gordon, *Science* **365**, 605 (2019).
 - ⁴² T. Maier, M. Jarrell, T. Pruschke, and M. H. Hettler, *Rev. Mod. Phys.* **77**, 1027 (2005).
 - ⁴³ L. de' Medici, S. R. Hassan, M. Capone, and X. Dai, *Phys. Rev. Lett.* **102**, 126401 (2009).
 - ⁴⁴ W.-C. Lee and T.-K. Lee, *Phys. Rev. B* **96**, 115114 (2017).